

CHAPTER 4

Copper oxide nanostructure for dye-sensitized solar cell application

A solar cell or photovoltaic cell is a device that converts light energy into electrical energy. The term solar cell is reserved for devices intended specifically to capture energy from sunlight, while the term photovoltaic cell is used when the source is unspecified. Fundamentally, the device needs to fulfill only two functions; photo-generation of charge carrier (electrons or holes) in a light absorbing material and separation of the charge carriers to a conductive contact that will transmit the electricity. This conversion is called the photovoltaic effect, and the field of research related to solar cells is known as photovoltaic.

Dye-sensitized solar cells (DSSCs) are one new choice for solar energy applications. Previously, a solar cell is a device that is made from semiconductor materials such as silicon, gallium arsenide, indium phosphide, cadmium telluride and copper indium diselenide, etc. that absorbs sunlight and converts it into electrical carriers, then separates electrons and holes to produce energy at positive/negative junctions. If the positive and negative junctions of solar cell are connected to DC electrical equipment, work is done. Solar cells have different types of design such as single crystalline, polycrystalline, multicrystalline and amorphous, etc. Solar cells have photoconversion efficiencies varying from 6% for amorphous, silicon-based solar cells to 42.8% with multiple-junction research lab cells. Solar cells for

commercially available multicrystalline Si solar cells have efficiency around 14-16%. The highest efficiency cells have not always been the most economical for example a 30% efficient multi-junction cell based on exotic materials such as gallium arsenide or indium selenide and produced in low volume might well cost one hundred times as much as an 8% efficient amorphous silicon cell in mass production, while only delivering about four times the electrical power.

DSSCs are a metal-oxide wide-band-gap solar cell composed of a dye-modified wide band gap semiconductor photoelectrode, the dye molecules adsorbed on the surface of the wide band gap semiconductor photoelectrode, a counterelectrode and an electrolyte containing a redox couple between photoelectrode and counterelectrode. The major research on DSSCs has made by the Grätzel group.⁽²³⁾ They have obtained promising results with photoconversion efficiency up to 10.8% as reported several years ago.⁽²⁴⁾ Nowadays, the DSSC based on TiO_2 is widely investigated. Recently, investigation of ZnO as an alternative photoelectrode has been intensively carried out due to its band gap, electron affinity, and electron injection efficiency which are nearly the same as TiO_2 . However, the photoconversion efficiencies of DSSCs based on ZnO are relatively low. Several methods have been applied to improve the photoconversion efficiencies of ZnO DSSCs⁽²⁵⁾. Formation of a p-n junction electrode is one of the methods that are used to improve the performance of ZnO DSSCs⁽²⁶⁾. For example, Bandaranayake and co-workers⁽²⁷⁾ have fabricated a p-n junction electrode for minimizing the charge recombination in DSSCs. They found that the efficiency of the TiO_2 DSSC can be improved and they have observed an open circuit voltage of about 730 mV, a short circuit current of about 16.7 mA, a fill factor of 0.66, and a photoconversion efficiency of 7.74%. Some

study was prepared with p-type counterelectrode and p-n junction for used as application in solar cells.

4.1 Literature review of CuO nanostructures for dye-sensitized solar cell applications

4.1.1 CuO nanostructures as a cathode in dye-sensitized solar cells

Anandan and co-workers⁽²⁸⁾ synthesized CuO nanorod arrays in situ on a copper electrode for use as a cathode in DSSCs. The advantages of their method include low temperature process, uniform size, superior adherence, and homogeneous coverage. The effects of the solution pH on the CuO nanorod growth have been studied, and better nanorod films appear to grow at relatively high pH values. Overall energy conversion efficiency up to 0.29% has been obtained. This initial result is quite promising considering that further optimization of the photovoltaic performance is possible. The prepared CuO nanorods and solar cell results are shown in figure 4.1 and 4.2, respectively.

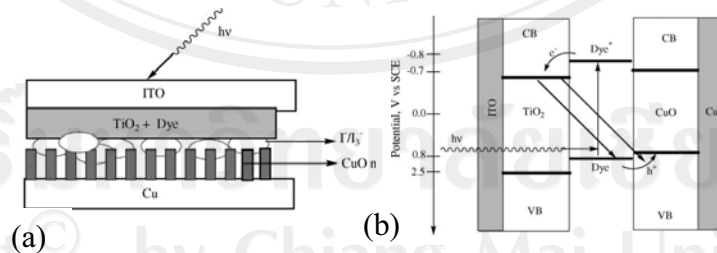


Figure 4.1 (a) Schematic illustration of the dye-sensitized photovoltaic cell [ITO/TiO₂/dye/E/CuO/Cu], in which p-CuO semiconductor nanorods are used. (b) Schematic energy level diagram showing the band structure alignment and photoinduced charge separation in the photovoltaic cell in (a) (the energy level positions are approximated)⁽²⁸⁾.

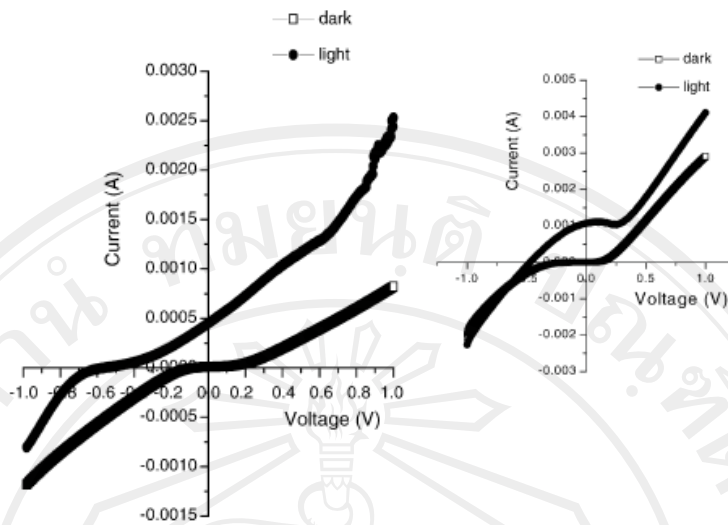


Figure 4.2 Current (I)–voltage (V) characteristics of the dye-sensitized solar cell of the type [ITO/TiO₂/dye/E/CuO/Cu] in the presence and absence of light, where the p-CuO nanorods act as a hole-conducting medium. Inset shows I–V curves for the dye-sensitized solar cell of the type [ITO/TiO₂/dye/E/Pt/ITO] ⁽²⁸⁾.

Liu and co-workers ⁽²⁹⁾ have investigated the fabrication of nanostructure CuO films for DSSCs using a wet-chemical method at different pH values, reaction temperatures and time durations. Measurements show: nanoflake is much better for getting higher energy efficiency than nanorod. Maybe nanoflake has stronger ability to absorb electrolyte than nanorod. The as-prepared nanostructured CuO films were tested as cathodes for dye-sensitized solar cells. It was found that with high water bath temperature, we can get more stable and relatively high short circuit current and open circuit voltage, then high solar energy conversion efficiency. This demonstrates that the nanostructured CuO films are a promising cathode material for DSSCs due to the reasonably good photovoltaic efficiency, low cost and non-toxicity to the environment. They found that the energy conversion efficiency of the solar cells using

the nano-CuO film cathode is correlated with the capacitance of the CuO film. The relatively low energy conversion efficiency is mainly caused by the low fill factor, which is in turn attributed to the relatively high intrinsic resistivity of the CuO film and/or the slow interfacial charge transfer. The use of the nanostructure CuO films as cathodes has opened a new avenue for research on dye-sensitized solar cells. Further studies are needed to improve the fill factor of the nano-CuO-cathode-based solar cells. The prepared CuO nanostructures I-V curves of DSSC are shown in figure 4.3.

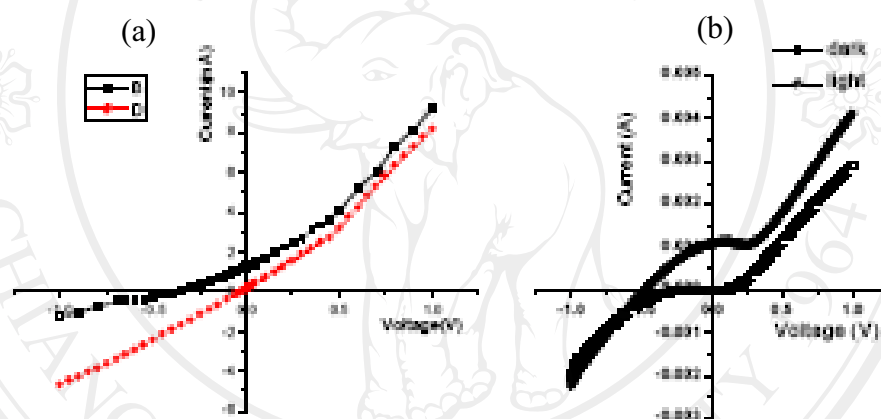


Figure 4.3 I-V curves of (a) a dye-sensitized solar cell of the type [ITO/TiO₂/dye/E1/CuO(nanoflake)/Cu] in the presence and absence of light, where the CuO film (prepared at pH 11.8, 90°C, 80 h) acts as a hole transport medium and (b) a reference solar cell [ITO/TiO₂/dye/E1/Pt]⁽²⁹⁾.

4.1.2 p-n junction device of CuO in application of photodevice

Tripathi and co-workers⁽³⁰⁾ synthesized a nanostructured TiO₂-CuO admixed photoelectrode and researched its use as a photoelectrode for high-efficiency photoelectrochemical (PEC) solar cells for hydrogen production. In addition to TiO₂, the photoelectrode corresponding to n-type TiO₂-CuO was also prepared for obtaining

improved spectral response. Copper oxide was deposited on the above-mentioned n-type TiO_2 -coated photoelectrode by employing a chemical vapor deposition technique. This electrode was also annealed in oxygen ambient at 500°C . The structural behavior and PEC behavior of both cells, i.e., ns- TiO_2 and ns- TiO_2 -CuO PEC were investigated by different experimental tools. The CuO admixed ns- TiO_2 exhibited a high photocurrent and photovoltage of 18.6 mA/cm^2 and 680 mV . The n-type TiO_2 -CuO electrode exhibited a higher hydrogen gas evolution rate of 14.00 l/nm^2 . The schematic diagram of SC-SEP PEC cell was shown in figure 4.4.

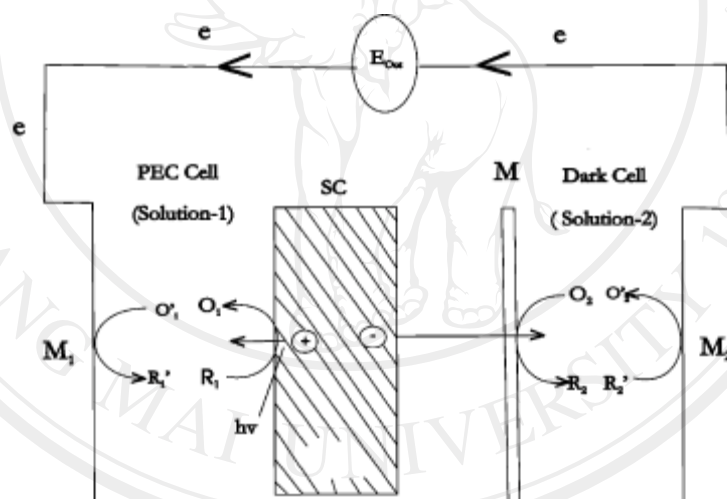


Figure 4.4 Schematic diagram of SC-SEP PEC cell⁽³⁰⁾.

Vigil and co-workers⁽³¹⁾ studied deposition of copper oxide in a porous TiO_2 layer using a very simple photochemical method. Sample irradiation was performed at room temperature using an aqueous solution of copper formate for deposition. Therefore, the proposed technique is in line with green chemistry practice. TiO_2 layers were irradiated while immersed in a 4 mM copper formate precursor solution, i.e., in a condition for which solute is not limited (infinite). For this condition, according to X-

ray diffraction and SEM images, nanocrystals of Cu and copper oxide were formed. To avoid crystals nucleation, samples were first immersed in the precursor solution and then irradiated. In this condition, for all concentrations used the number of copper ions was smaller than the available sites to bind on the nanoporous TiO₂ real surface. Relatively large crystals of copper (II) hydroxide hydrate (Cu(OH)₂·H₂O) were formed when using 160 mM copper (II) formate precursor solution. For 4 mM concentration and 40 mM concentration, neither crystals of Cu, nor Cu₂O, nor (Cu(OH)₂·H₂O) were detected using SEM and XRD despite transmission spectra showing Cu₂O absorption. Photocurrent was obtained for TiO₂/copper oxide samples used as photoelectrodes in a two electrode photoelectrochemical cell. Direction of current flow shows electron injection from the copper oxide to the TiO₂ without applying bias. Spectral photocurrent analysis showed that electrons are also injected to the TiO₂ for photon energies lower than Cu₂O energy band gap. This indicates the existence of lower energy states created at the TiO₂/copper oxide interface and it needs further study.

4.1.3 p-n junction DSSC

To improve the efficiency of DSSCs some researcher studied p-n junction to decrease the recombination rate of electron from valance band of semiconductor to LUMO of dye.

Bandara and co-workers⁽³²⁾ fabricated p-n junction electrodes made of n-type SnO₂ and p-type NiO for control of charge recombination in DSSCs, p-n junction electrode were fabricated by coating nanocrystalline a SnO₂ thin film with a thin layer of p-type NiO which was found to increase the sensitized photocurrent and photovoltage. In the first method, SnO₂ thin films were first prepared by spray

pyrolysis and immersed in Ni_2^+ solution. In the second method, SnO_2 colloid and Ni_2^+ were mixed in an agate and thin films were fabricated by doctor blade method. Films deposited on CTO glass plates were coated with the dye cisdithiocyanato [N-bis(2-20-bipyridyl-4,40-dicarboxylic acid)] Ru(II) by immersing the plates in a warm (80°C) alcoholic solution ($3.0 \times 10^{-3}\text{M}$) of this dye for 4 h. After rinsing the plate with acetonitrile and drying, the cell was formed by clamping the dyed film surface to the counter-electrode (lightly platinized CTO glass plate) and filling the capillary space with the electrolyte (0.6M dimethylpropyl imidazolium iodide+0.1M LiI+0.05M I_2 +0.5M t-butyl pyridine in methoxy-acetonitrile). It can be concluded the efficiency of the DSSC SnO_2 solar cells can be improved by coating a thin layer of p-type NiO. The p-n junction formed between SnO_2 and NiO facilitate the efficient electron transfer. In addition to the junction behaviour, NiO acts as a barrier for charge recombination leading to higher IPCE. Such p-n junction solar cells work better if the dye adsorption occurs on the p-type oxide. Figure 4.6 shows schematic diagram illustrating the energy levels of SnO_2 , NiO and the ground and excited energy levels of the Ru-dye.

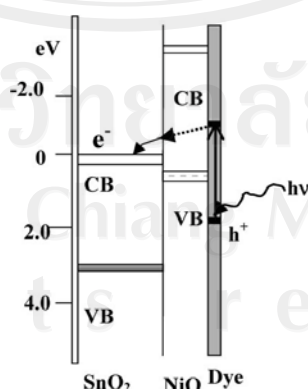


Figure 4.5 Schematic diagram illustrating the energy levels of SnO_2 , NiO and the ground and excited energy levels of the Ru-dye⁽³²⁾.

Bandara and co-workers⁽³³⁾ have investigated p-n junction electrodes made of n-type TiO₂ and p-type MgO for sensitized degradation of colorants in aqueous phase. The results indicate that both dye adsorption amount and the equilibrium constant increase after coating TiO₂ with an MgO layer and the photocatalytic activity is highly dependent on the thickness of the MgO layer. In this report, using charge transfer studies, they propose that the dye adsorption amount might not be the rate-limiting step, but the slow charge recombination on TiO₂/MgO leads to higher dye degradation on TiO₂/MgO composite catalyst. They show that the MgO layer on TiO₂ retards the charge recombination resulting in higher dye degradation in the absence of a suitable redox couple. It was shown that the thin layer of insulating MgO on TiO₂ acts as a barrier for charge recombination and charge recombination rates were progressively reduced with the MgO amount present on TiO₂. Therefore, the promoting effect of MgO layer on TiO₂ could also be attributed to slow charge recombination in addition to enhanced dye adsorption amount. A schematic presentation of electron transfer process is shown in figure 4.5.

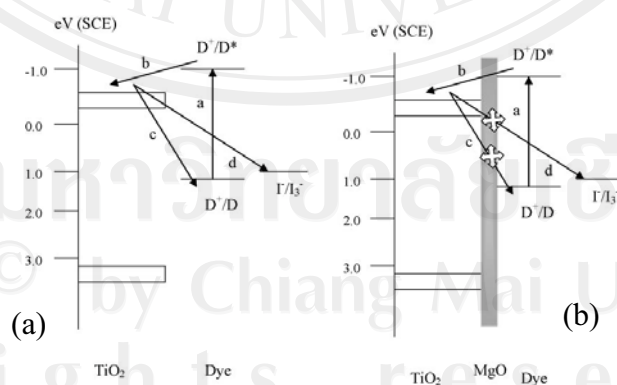


Figure 4.6 A schematic presentation of electron transfer process for (a) TiO₂/dye, (b) TiO₂/MgO/dye; (a) absorption of light by the dye, (b) injection of excited electron of dye in to the CB of TiO₂, (c and d) regeneration of dye (back reactions)⁽³³⁾.

4.1.4 CuO as photoelectrode in DSSCs

Sumikura and co-workers⁽³⁴⁾ prepared nanoporous p-type CuO semiconductor electrodes adsorbing various dyes with different HOMO levels and anchoring groups. Solar cells were fabricated by coupling each of the dyed electrodes with a platinum counter electrode and filled with electrolytes containing Γ/I_3^- redox couple. Cathodic photocurrent due to hole injection from the adsorbed dye to the semiconductor was observed. Only the dyes with HOMO and LUMO potentials more positive than valence band (VB) and conduction band (CB) edges, respectively, functioned as sensitizers for p-type DSSCs. Effects of annealing temperature and thickness of the CuO nanoporous membrane on cell performance were investigated as well. Figure 4.8 shows J–V characteristics of p-DSSCs using CuO electrodes dyed with four different dyes and an undyed CuO electrode. Irradiation intensity was $100\text{mW}/\text{cm}^2$. Figure 4.9 shows IPCE define of p-DSSCs using CuO electrodes dyed with four different dyes and an undyed CuO electrode. Figure 4.9 are absorption spectra of each dyed and undyed nanoporous CuO electrode. CuO film thickness is 0.34, 0.41, 0.52, 0.42 and $0.36\ \mu\text{m}$ for Fast Green FCF dye, NK-3628, NK-2612, N3 and without dye, respectively. Figure 4.10 shows energy diagram of the dyes and CuO.

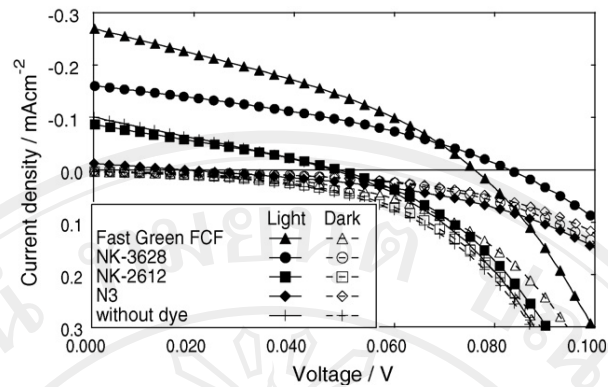


Figure 4.7 I–V characteristics of p-DSSCs using CuO electrodes dyed with four different dyes and an undyed CuO electrode. Irradiation intensity was $100\text{mW}/\text{cm}^2$ ⁽³⁴⁾.

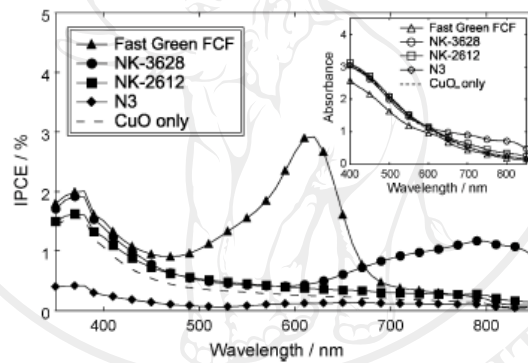


Figure 4.8 IPCE of p-DSSCs using CuO electrodes dyed with four different dyes and an undyed CuO electrode. Inset shows absorption spectra of each dyed and undyed nanoporous CuO electrode. CuO film thickness is 0.34, 0.41, 0.52, 0.42 and 0.36 μm for Fast Green FCF dye, NK-3628, NK-2612, N3 and without dye⁽³⁴⁾.

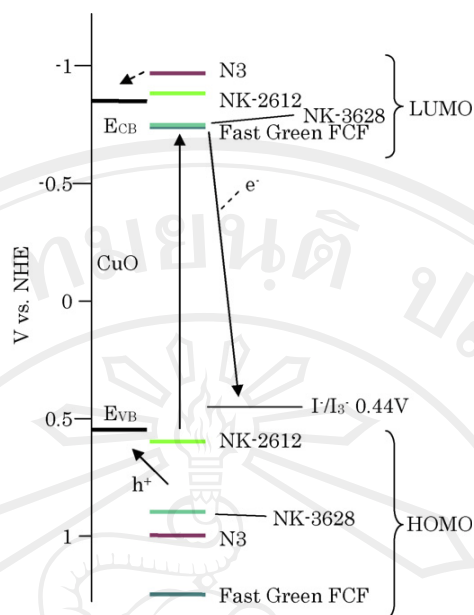


Figure 4.9 Energy diagram of the dyes and CuO⁽³⁴⁾.

4.1.5 Passivating layer for improving efficiency of DSSCs

Hossain and co-workers⁽³⁵⁾ studied the effect of sputter-deposited TiO₂ passivating layer on the performance of dye-sensitized solar cells based on sol-gel derived photoelectrode. A thin passivating TiO₂ under layer was deposited on SnO₂:F coated glass substrate by facing target sputtering technique with different sputtering pressures: 0.1, 1.0 and 2.0 Pa. An upper nanoporous TiO₂ layer was deposited by conventional sol-gel technique with polyethylene glycol. The schematic diagrams of DSSCs with TiO₂ passivating layer are shown in figure 4.11. The variation of photoelectric conversion efficiency of the solar cells with different TiO₂ passivating layers is discussed with the analysis of crystallographic and microstructural properties of passivating and upper nanoporous TiO₂ layers. The observed crystalline phase-difference between the passivating layer (anatase and rutile) and upper TiO₂ electrode (anatase) has an important effect on smooth electron movement due to the suitable

energy band potentials. J-V characteristics for the DSSCs were shown in figure 4.12 and table 4.1 shows photovoltaic performances of all the DSSCs. The observed crystalline phase-difference between the passivating layer (anatase and rutile) and upper TiO₂ electrode (anatase) has an important effect on smooth electron movement due to the suitable energy band potentials.

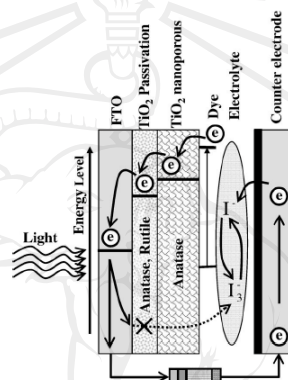


Figure 4.10 Schematic diagrams of dye-sensitized solar cells with TiO₂ passivating layer⁽³⁵⁾.

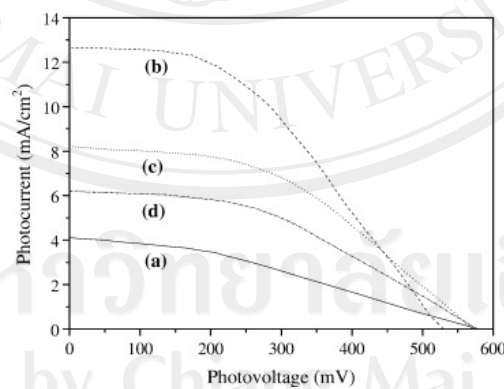


Figure 4.11 J-V characteristics for the DSSCs based on nanoporous TiO₂ electrodes (a) without passivating layer and with passivating layer of sputtering pressure at (b) 0.1 Pa, (c) 1.0 Pa and (d) 2.0 Pa⁽³⁵⁾.

Table 4.1 Photovoltaic performances of all the DSSCs with and without passivating layer based on TiO₂ electrode ⁽³⁵⁾.

DSSCs	η (%)	FF	J_{SC} (mA/cm ²)	V_{OC} (mV)
Without passivating layer	0.79	33	4.1	580
With passivating layer of 0.1 Pa	2.85	43	12.7	530
With passivating layer of 1.0 Pa	2.07	44	8.2	571
With passivating layer of 2.0 Pa	1.51	42	6.2	600

4.2 Experimental of dye-sensitized solar cell applications

4.2.1 Solar cells measurement

Light of different wavelengths is absorbed to different depths in a wide band gap semiconductor film. The spectral response (photovoltaic action spectrum) of a device is determined by the photocurrent at various wavelengths relative to the number of photons of a particular wavelength incident on the device. The band energy diagram of a DSSC is shown in figure 4.13. The effectiveness of a solar cell to convert incident photons of a given wavelength into photocurrent is measured by the incident monochromatic photon to current conversion efficiency (IPCE) as defined by

$$IPCE\% = 1240 \frac{J_{sc}}{\lambda P_{in}} \quad (4.1)$$

where J_{sc} is the short-circuit current density (mA/cm²), λ is the excitation wavelength (nm), and P_{in} is the incident photon flux (W/m²).

The photocurrent, photovoltage and photoconversion efficiency characteristics for DSSCs were measured under illumination of simulated sunlight from a solar simulator with radiant power of 100 mW/cm² (Photovoltaic Cell Testing Light Source Model 16S-002 300 watt Model 16S-002-150-AM1.5, 150-watt AIR MASS Solar Simulator, 2.4 inch (6 cm) horizontal round beam, AMO & AM1.5 filters, full

spectrum spectral range: 290 to 2800nm as per graph shown in the literature, includes 150-watt xenon lamp, Approx. Intensity 600 W/m^2 at 18 inches from lens & XPS200 power source in 115/230V 50-60Hz.). The incident light intensity was calibrated with standard Si solar cell. The photocurrent densities versus photovoltage (J–V) characteristics were measured with dc voltage and current sources interfaced and controlled by computer. The shot current density (J_{SC}), open circuit voltage (V_{OC}) and efficiency (η) were determined from the J–V curve. The incident light intensity was calibrated with a reference solar cell produced by Fraunhofer ISE. All measurements of photovoltaic performances were undertaken in normal atmosphere. The measurements were made a day after the cell preparation and the average of three consecutive measurements were taken. No further long-term stability test has been done. For each J–V measurement, the ZnO DSSC prepared at the same batch was simultaneously measured as a reference cell.

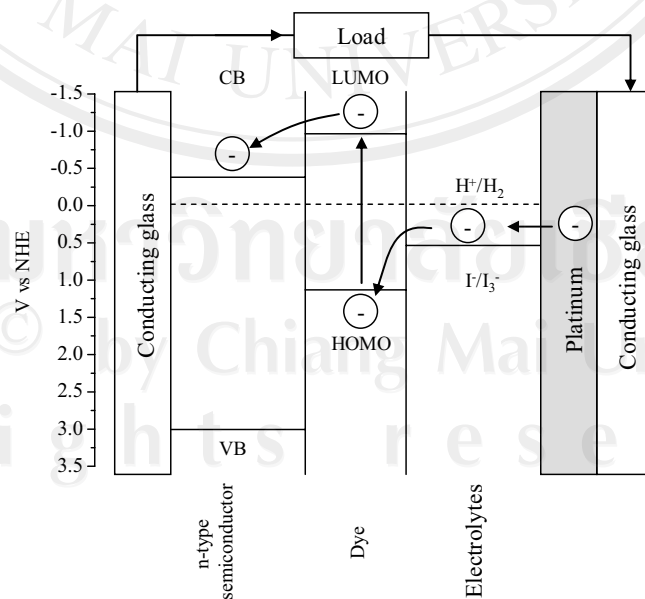


Figure 4.12 Schematic energy diagram for a DSSC.

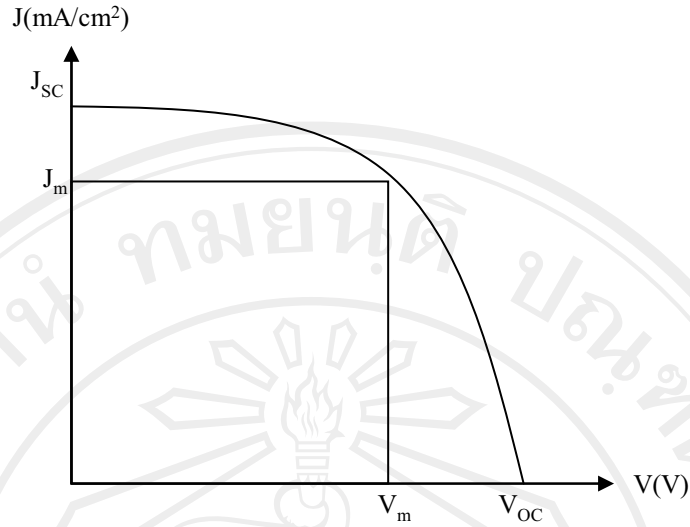


Figure 4.13 J-V curve of a solar cell under illumination displaying the current density and voltage J_{\max} and V_{\max} , respectively, at maximum power.

Figure 4.13 shows a typical J-V characteristics of a measured DSSC under illumination. The fill factor (FF) of the solar cell is a measure of the realizable power from the cell. It is defined as

$$FF = \frac{J_m V_m}{J_{sc} V_{oc}} \quad (4.2)$$

where V_m is the voltage (V) at which the maximum power is delivered and J_m is the corresponding current density, J_{sc} is the short-circuit current density, and V_{oc} is the open-circuit voltage (V). The power conversion efficiency is also another important parameter that characterizes a solar cell. It is defined as

$$(\eta)\% = \frac{J_m V_m}{P_{in}} \times 100 \quad (4.3)$$

or

$$(\eta)\% = FF \left(\frac{J_m V_m}{P_{in}} \right) \quad (4.4)$$

where P_{in} is the incident photon flux usually measured in watt per centimeter-square. Both parameters are determined from the J–V characteristics of the device under illumination. The equivalent circuit for a single junction solar cell is shown in figure 4.14.

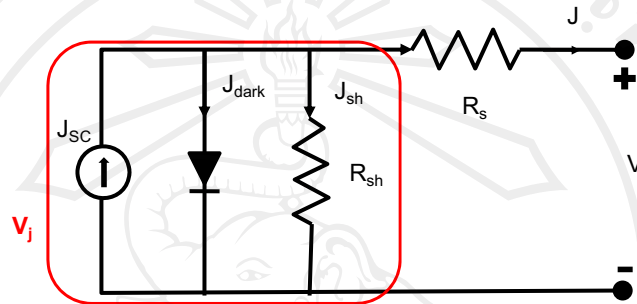


Figure 4.14 Equivalent circuits for a single junction solar cell. The photogenerated current J_{SC} shows in the inverse direction of the diode. Shunt resistance R_{sh} and series resistance R_s are important for the fill factor. Ideally, series resistance should be low and shunt resistance should be high.

From figure 4.15 the current density of DSSCs is

$$J = J_{SC} - J_{dark} - J_{sh} \quad (4.5)$$

where

J is output current density (A/cm^2)

J_{SC} is short-circuit photo current density (A/cm^2)

J_{dark} is diode current density or dark current density (A/cm^2)

J_{sh} is shunt current density (A/cm^2)

And the voltage of DSSCs is

$$V_j = V + J R_S \quad (4.6)$$

where

V is voltage across the output terminals (V)

J is output current density (A/cm^2)

R_S is series resistance ($\Omega\text{-cm}^2$)

By the Shockley diode equation, the current diverted through the diode is:

$$J_{\text{dark}} = J_0 \left\{ \exp \left[\frac{qV_j}{nkT} \right] - 1 \right\} \quad (4.7)$$

where

J_0 is reverse bias saturation current density (A/cm^2)

n is diode ideality factor (1 for an ideal diode)

q is elementary charge

k is Boltzmann's constant

T is absolute temperature

By Ohm's law, the current diverted through the shunt resistor is:

$$J_{\text{sh}} = \frac{V_j}{R_{\text{sh}}} \quad (4.8)$$

where R_{sh} is shunt resistance (Ω)

The values of J_0 , R_S , and R_{sh} are dependent upon the physical size of the solar cell.

$$J = J_{\text{SC}} - J_0 \left\{ \exp \left[\frac{q(V+J R_S)}{nkT} \right] - 1 \right\} - \frac{V+J R_S}{R_{\text{sh}}} \quad (4.9)$$

where J is current density (A/cm^2)

J_0 is reverse saturation current density (A/cm^2)

R_S is specific series resistance ($\Omega\text{-cm}^2$)

R_{sh} is specific shunt resistance ($\Omega\text{-cm}^2$)

The meaning of R_S and R_{sh} can be expressed as

R_S arises from the resistance of the cell materials to current flow, particular through the front surface contacts and resistive contacts.

R_{sh} arises from leakage of current through the cell, around the edges of the device and between contacts of different polarity.

4.3 Preparation of DSSCs

CuO nanostructures were used in DSSCs in this study. There are three types of DSSCs prepared as shown in schematic diagram of DSSCs in figure 4.16. The first type used ZnO as photoelectrode with CuO nanostructure as counterelectrode, the second type used ZnO as photoelectrode with Pt as counterelectrode and the third type used ZnO and CuO nanostructure as p-n junction photoelectrode with Pt as counterelectrode. For discussion schematic diagram of DSSC structures used symbol as photoelectrode-counterelectrode.

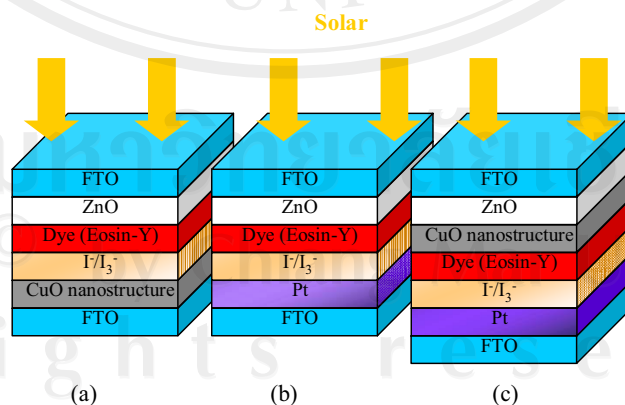


Figure 4.15 Schematic diagram of DSSC structures with different photoelectrodes-counterelectrodes for (a) ZnO-CuO nanostructure, (b) ZnO-platinum, and (c) ZnO/CuO nanostructure-platinum.

4.3.1 ZnO as n-type photoelectrode

ZnO is a wide bandgap semiconductor (3.37 eV) which is one of the ideal materials to be used as the photoelectrode for DSSCs. This is due to its band gap, electron affinity, and electron injection efficiency which are nearly the same as titanium dioxide (TiO₂). The ZnO semiconductor is used only for receive a charge separation or the photoelectrons from a separate photosensitive dye. Additionally the charge separation is not provided by the ZnO semiconductor. Since the dye molecules are quite small, in order to capture a reasonable amount of the incoming light the layer of dye molecules needs to be made fairly thick, much thicker than the molecules themselves. To address this problem, a nanostructure material is used as a scaffold to hold large numbers of the dye molecules in a 3-D matrix to increase the number of molecules and the surface area of the cell. In existing designs, this scaffolding is provided by the semiconductor material, which serves double-duty. Energy levels of a semiconductor can be discussed using figure 4.16. Semiconductors have energy band level such as VB, CB level and Fermi level energy (E_F) of semiconductor in vacuum as shown in figure 4.17.

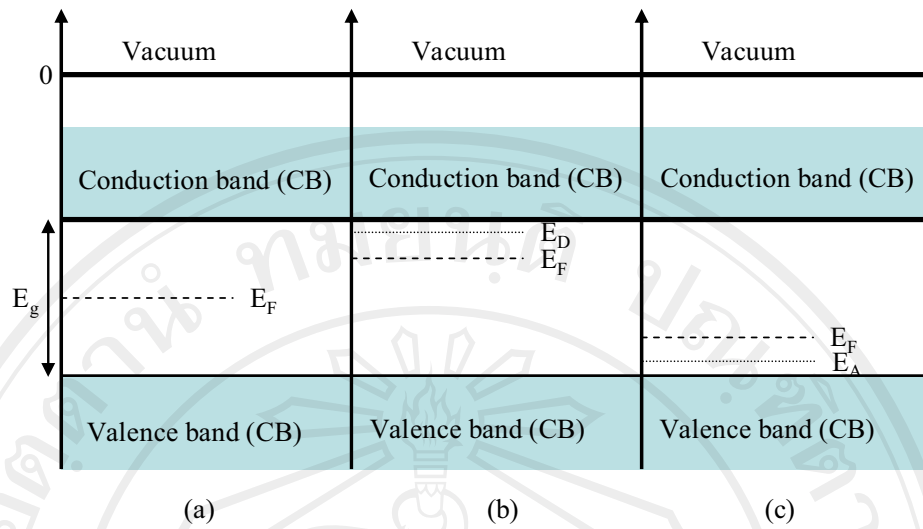


Figure 4.16 Energy band diagrams of (a) intrinsic, (b) n-type semiconductor and (c) p-type semiconductor in vacuum.

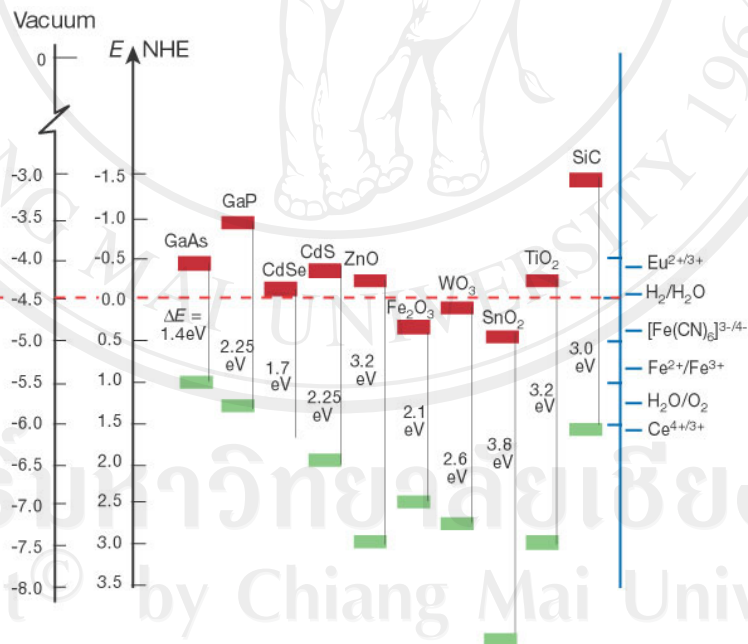


Figure 4.17 Band positions of several semiconductors in contact with aqueous electrolyte at pH 1⁽³⁶⁾.

The energy positions of the band edges are shown both on the absolute vacuum scale (AVS) and with respect to the normal hydrogen electrode (NHE) and can be related by

$$E(\text{AVS}) = - E(\text{NHE}) - 4.5 \quad (4.10)$$

In ZnO DSSC construction, the top layer is a transparent anode made of fluorine-doped tin oxide ($\text{SnO}_2:\text{F}$, FTO with a sheet resistance of $8 \Omega/\text{square}$) conducting glass deposited on the back of a glass plate. On the back of the conductive plate is a thin layer of ZnO semiconductor nanostructure, which forms into a highly porous structure with an extremely high surface area. The plate is then immersed in a mixture of a photosensitive dye and a solvent. After soaking the film in the dye solution, a thin layer of the dye is left covalently bonded to the surface of the ZnO. A separate backing is made with thin layer of the iodide electrolyte spread over a conductive sheet, typically platinum metal. The front and back parts are then coupled and sealed together to prevent the electrolyte from leaking. The construction is simple enough that there are hobby kits available for hand-constructing them. Although they use a number of "advanced" materials, these are inexpensive compared to the silicon needed for normal cells because they require no expensive manufacturing steps.

In operation, sunlight or photon energy enters the cell through the transparent FTO glass top contact, striking the dye on the surface of the ZnO. Photons striking the dye with enough energy to be absorbed will create an excited dye from ground state (Highest occupied molecular orbital, HOMO) to the excited state (lowest unoccupied molecular orbital, LUMO), an electron filled in the LUMO can be "injected" directly into the conduction band of the ZnO, and from there it moves by a chemical diffusion gradient to the clear anode on top. Meanwhile, the dye molecule has lost an electron

and the molecule will decompose if another electron is not provided. The dye strips one from iodide in electrolyte below the ZnO, oxidizing it into triiodide. This reaction occurs quite quickly compared to the time that it takes for an injected electron to recombine with the oxidized dye molecule, preventing this recombination reaction that would effectively short-circuit the solar cell. The triiodide then recovers its missing electron by mechanically diffusing to the bottom of the cell, where the counter electrode re-introduces the electrons after flowing through the external circuit.

4.3.2 Standard photoelectrode for ZnO DSSCs

The photoelectrode of standard ZnO DSSCs was prepared by using ZnO powder (Aldrich, 99.9%) which was screened on conducting glass sheets by using screening technique method with area 0.5×2 cm, thickness around 10 μm ; ZnO powder was dissolved in polyethylene glycol (PEG) to form ZnO paste and heated at 400°C for 1 hr under normal atmosphere to remove PEG. The ZnO photoelectrode was soaking in solution of dye for dye absorption on ZnO.

4.3.3 Sputtering of ZnO passivating layer for photoelectrode

ZnO passivating layer was prepared by rf-magnetron sputtering technique on FTO. This ZnO passivating layer was used as a blocking layer at the interface of FTO and electrolyte to improve the efficiency of the DSSCs. The sputtering times were varied to 5, 10, 20, and 40 minute with fixed distance between FTO substrate and ZnO target of 60 mm. A sputtering ZnO target has diameter of 100 mm and purity of 99.9%. For sputtering conditions, the base pressure was 5×10^{-5} Torr, the deposition pressure was 25 mTorr under argon atmosphere by using an rf power of 200 W. During deposition of ZnO, there is no heating to the FTO substrate. After sputtering process, the ZnO passivating layer was characterized by scanning electron

microscopy (SEM) for morphology. The next ZnO layer was prepared by screening ZnO paste on the ZnO passivating layer with thickness of 30 μm . ZnO paste were prepared by mixing ZnO powder with polyethylene glycol (PEG) ratio 1:1 by weight then the mixed solution was stirred for 1 h to form as ZnO paste. After screening the samples were heat at 400°C for 1 h. to remove PEG.

Table 4.2 Preparation of photoelectrode

Type code	ZnO sputtering time (min)	With CuO thin films as a barrier layer
ZnO	-	-
A05	5	-
A10	10	-
A20	20	-
A40	40	-
B00	-	Yes
B05	5	Yes
B10	10	Yes
B20	20	Yes
B40	40	Yes

4.3.4 CuO barrier layer photoelectrode

Barrier layer photoelectrodes were prepared by using 3 types of CuO such as CuO powder, CuO nanowires and CuO thin films as p-type photoelectrod by coating onto the ZnO photoelectrode (discuss in 4.3.2). The process for coating different types of CuO onto ZnO substrate is as follows. For CuO powder, the CuO powder was dissolved in PEG to form CuO paste then screened CuO paste on ZnO photoelectrode and heated at 400°C for 1 hr under normal atmosphere to remove PEG. For CuO nanowires, the Cu powder was dissolved in PEG to form Cu powder paste and followed by screening copper powder paste on ZnO photoelectrode then heated at 400°C for 1 hr under normal atmosphere to remove PEG. After that heated at 400°C for 6 hr under normal atmosphere to oxidize copper to CuO nanowires by oxidation

reaction.; for CuO thin films, ZnO photoelectrode was load into evaporation chamber as a substrate and Cu powder was placed in heating coil at vacuum of 0.4 mTorr. Then copper thin films were deposited onto the photoelectrode substrate in a vacuum tube, the distance between the electric boat and the substrate surface was 7 cm. The temperature of substrates was keeping at room temperature. The coated photoelectrode was loading into furnace and heat at 400°C for 6 hr to oxidize Cu thin films to CuO thin films by oxidation reaction. The morphology of the complete photoelectrodes was investigated by FE-SEM.

For improving efficiency of the solar cell, CuO thin films were used as barrier layer in the photoelectrode. The CuO thin film was prepared by thermal evaporation of copper powder onto the ZnO layer with distance from the substrate to the copper powder in the heating electric boat of 7 cm. Then the copper thin film on the ZnO substrate was heated under normal atmosphere at 400°C for 6 h for oxidation reaction to CuO. The morphology of the photoelectrode was investigated by field emission scanning electron microscopy (FE-SEM). Table 4.2 shows the prepared conditions of the many photoelectrodes.

4.3.5 Platinum counterelectrode

Conventional platinized counterelectrode of DSSCs was prepared by various methods such as electrochemical deposition, sputtering and thermal decomposition. But electrodes prepared by these methods have high platinum loadings which were not in accordance with the character of low costing of DSSCs. To reduce the fabrication cost of the counterelectrodes, several other types of counter electrodes have been reported such as carbon materials based counter electrodes with sufficient conductivity as an attractive low cost substitute for the platinum. Saito and co-

workers⁽³⁷⁾ used chemically polymerized poly (3,4-ethylenedioxythiophene) on a conductive glass as a counterelectrode. However, the conversion efficiencies of the DSSCs based on carbon counter electrodes were lower than that based on the platinized counter electrode⁽³⁸⁾. The platinum counterelectrode used in this study was prepared from solution of platinum.

4.3.6 CuO counterelectrode

Two types of CuO counterelectrodes were used in this experiment: CuO powder and CuO nanowires. A CuO powder counterelectrode was fabricated by using a screen painting technique. CuO powder was dissolved in polyethylene glycol (PEG) to form CuO paste then the CuO paste was screened on conducting glass follow by heating at 400°C for 1 hr under normal atmosphere for remove PEG. Similarly, for CuO nanowires counterelectrode, Cu powder was dissolved in PEG to form copper paste then the Cu past was screened on FTO glass and heated at 400°C for 1 hr under normal atmosphere for remove binder follow by anneal at 400°C for 6 hr under normal atmosphere for oxidation reaction of Cu to be CuO nanowires. After heating the counterelectrodes were cooled down in the furnace.

4.3.7 Dye-sensitized solution

The dye-sensitized concept was invented in order to find a photoelectrochemical solar cell based on a semiconductor, which is stable against photocorrosion and yet absorb light in the visible region. Metal oxide semiconductor with wide band gap, most only absorbs UV-light. A way to extend their spectral response is to adsorb dye molecules absorbing visible light on the semiconductor surface: dye-sensitization. By the use of a porous network of nanometer-sized crystals of wide band gap semiconductor (e.g. TiO₂) deposited on a conducting glass substrate

(in this work used FTO as conducting glass substrate), the semiconductor surface can reach 100 time larger than the macroscopic area, per micrometer film thickness. The enlarged surface area of semiconductor leads to increased dye adsorption (by the same factor) resulting in an increased harvesting of sunlight and increased interface between the dye-sensitized semiconductor and the electrolyte.

Eosin is a fluorescent red dye resulting from the action of bromine on fluorescein. It is used to stain cytoplasm, collagen and muscle fibers for examination under the microscope. Efficient operation of DSSCs relies on both efficient electron injection and efficient dye regeneration. The LUMO energy level should be sufficiently higher than the conduction band edge minimum (E_{CB}) for efficient electron injection, and meanwhile the potential of the redox couple in the electrolyte (E_{redox}) should be higher than the HOMO energy level for efficient dye regeneration, which is key to the sustained photocurrent production. The maximum voltage of a DSSC under illumination corresponds to the difference of the E_f of semiconductor and the redox potential of the electrolyte.

Eosin-Y were purchased from Aldrich. Acetonitrile, electrolyte redox solution LiI, and I_2 were obtained from Wako Pure Chemical Industries Ltd. and used as receiver. The redox electrolytes used in this study were prepared in a dry box by dissolving weighted amounts of reagents in acetonitrile. The structural formula of Eosin-Y is shown in figure 4.18.

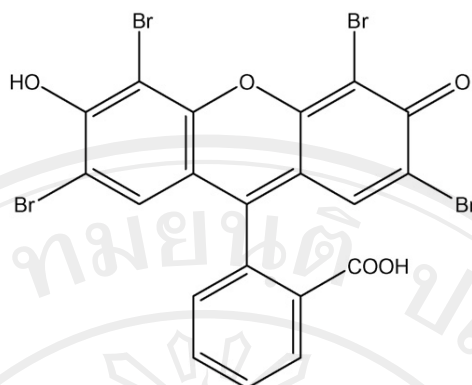


Figure 4.18 Structural formula of Eosin-Y⁽³⁹⁾.

4.3.8 DSSCs construction

DSSC structures with different photoelectrodes and counterelectrodes used in this experiment were shown as schematic diagram in figure 4.13 for (a) ZnO-CuO powder or nanowire, (b) ZnO-platinum, and (c) ZnO/CuO powder or nanowire-platinum. The photoelectrodes were soaked in Eosin-Y organic dye solution (0.04 g of Eosin-Y, $C_{20}H_6Br_4Na_2O_5$, in acetone 100 cm^3) for 24 h. The dye-loaded ZnO as photoelectrode and the Pt counterelectrode (0.5 mM Hydrogen hexachloroplatinate (IV) Hydrate, $C_{16}H_2Pt.aq$, in acetone solution) were assembled into a sealed device using a hot-melted double layer parafilm ($50\mu\text{m}$ thick). The redox electrolyte (0.3 M $LiI+0.03\text{ M } I_2$ in Polyethylene carbonate) was introduced into the inter-space between the photoelectrode and the counterelectrode through two predrilled holes on the side of the device.

4.4 Result of CuO nanostructure in DSSCs

4.4.1 Characterization of photoelectrode

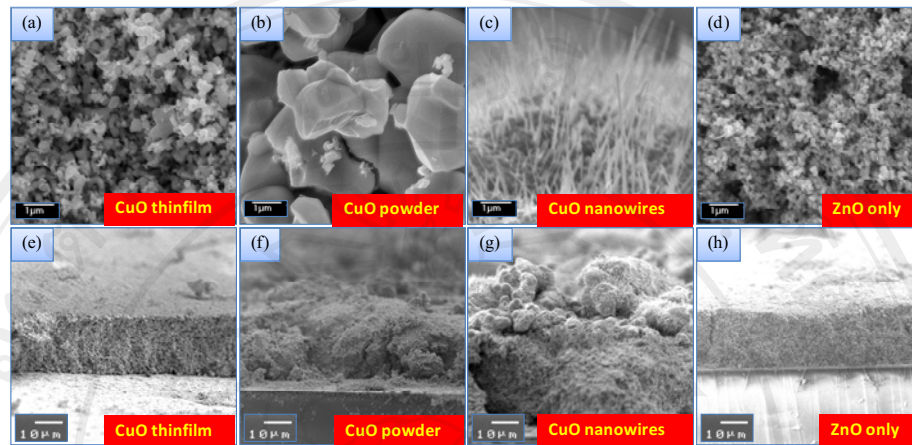


Figure 4.19 FE-SEM images of photoelectrodes: (a) ZnO powder/CuO thin film, (b) ZnO powder/CuO powder, (c) ZnO powder/CuO nanowires and (d) ZnO powder, (e), (f), (g) and (h) showed cross-section Fe-SEM images of ZnO powder/CuO thin film, ZnO powder/CuO powder, ZnO powder/CuO nanowires and ZnO powder, respectively.

Fig. 4.19 showed FE-SEM images of photoelectrodes: (a) ZnO powder/CuO thin films, (b) ZnO powder/CuO powder, (c) ZnO powder/CuO nanowires and (d) ZnO powder. The ZnO/CuO thin film exhibited similar morphology as ZnO powder which had microparticle structure with diameter of about 200–500 nm. However, the morphology of ZnO powder/CuO powder showed microparticle structure with large diameter of about 1–3 μm while the morphology of ZnO powder/CuO nanowires showed wire-like nanostructure on microstructure with diameter of about 50–200 nm and length of about 10 μm . It should be noted that the color of the copper powder and thin film turned into black color after the heating process indicating the phase change

to CuO. Fig. 4.19 (e), (f), (g) and (h) showed cross-section FE-SEM images of ZnO powder/CuO thin film, ZnO powder/CuO powder, ZnO powder/CuO nanowires and ZnO powder, respectively. The thickness of ZnO layer, CuO thin film, CuO nanowire and CuO powder obtained from cross-section FE-SEM images was about 20 μm , 1–3 μm , 10–20 μm , and 5–10 μm , respectively.

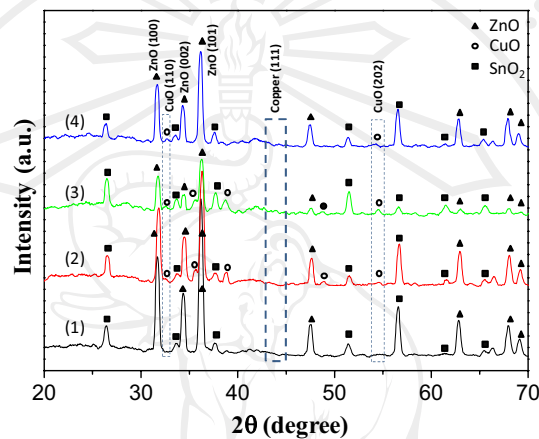


Fig. 4.20 This figure showed XRD pattern of (1) ZnO, (2) ZnO/CuO powder, (3) ZnO/CuO nanowire, and (4) ZnO/CuO thin film on FTO glass substrates.

Figure 4.20 showed XRD pattern of (a) ZnO, (b) ZnO/CuO powder, (c) ZnO/CuO nanowire, and (d) ZnO/CuO thin film on FTO glass substrates. For all cases, ZnO peaks and SnO₂ peaks from FTO were observed. It can be seen that CuO peaks were observed without copper peak for CuO layer cases indicating copper was completely oxidized to CuO.

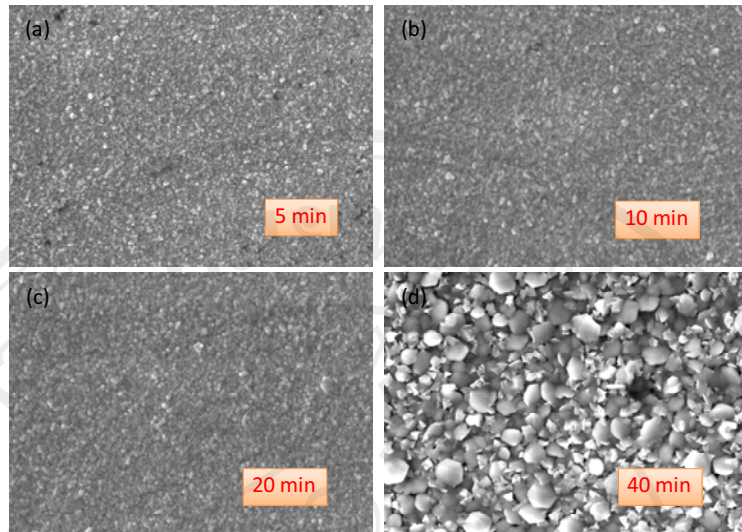


Figure 4.21 SEM images of ZnO passivating layer with sputtering time of (a) 5 minute, (b) 10 minute, (c) 20 minute and (d) 40 minute.

Figure 4.21 showed the morphology of ZnO passivating layer by SEM image of ZnO passivating layer with sputtering time of (a) 5 minute, (b) 10 minute, (c) 20 minute and (d) 40 minute. The dye absorption can discuss in case of ZnO passivating surface layer with difference morphology. The smaller size of ZnO passivating layer can absorb more dye than the larger size of ZnO passivating layer.

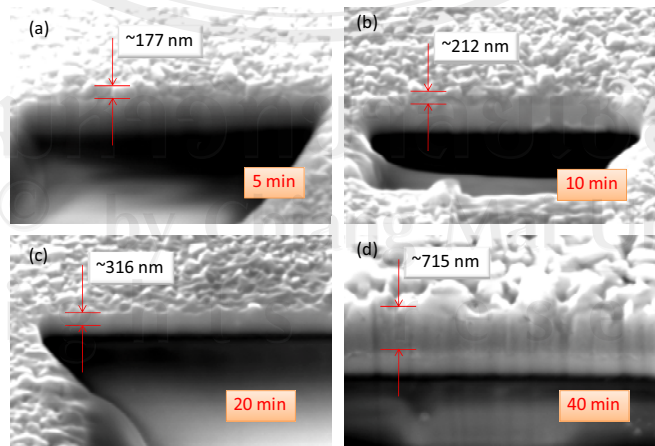


Figure 4.22 Cross-section SEM images of ZnO passivating layer by sputtering time of (a) 5 minute, (b) 10 minute, (c) 20 minute and (d) 40 minute.

Figure 4.22 showed cross-sectional SEM images of ZnO passivating layer at sputtering time of (a) 5, (b) 10, (c) 20 and (d) 40 minute. The thickness of ZnO passivating layer with sputtering time 5, 10, 20 and 40 was 177, 212, 316 and 715 nm, respectively. Usually, the thicker layer of ZnO passivating layer would have lower transparency.

4.4.2 CuO nanostructure as photoelectrode and counterelectrode

CuO was used as both photoelectrode and counterelectrode in DSSCs. Figure 4.23 shows J-V characteristic of ZnO DSSCs with CuO as a counterelectrode (line 4 and 5) and photoelectrode (line 1 and 2). For comparison, J-V characteristic of ZnO DSSCs without CuO (with Pt as a counterelectrode) is also shows in line 3 of Figure 4.23. The photoelectrochemical parameters such as short current density, open circuit voltage, fill factor and the overall photoconversion efficiency determined from the measured J-V curves are summarized in table 4.3. The efficiency with CuO as a counterelectrode shows lower efficiency than other solar cells. The solar cells with CuO used as both a photoelectrode and counterelectrode also show low efficiency. CuO used as a p-n junction photoelectrode shows higher efficiency than the standard cell (the cell with ZnO as a photoelectrode and Pt as a counterelectrode). The highest efficiency of this study was the solar cell with CuO nanowires used as a p-n junction in DSSCs (line 1) with efficiency of 0.46% and current density of 1.49 mA/cm^2 . This mean the CuO is optimization for used as a p-n photoelectrode in application of DSSCs (the DSSCs was not optimization).

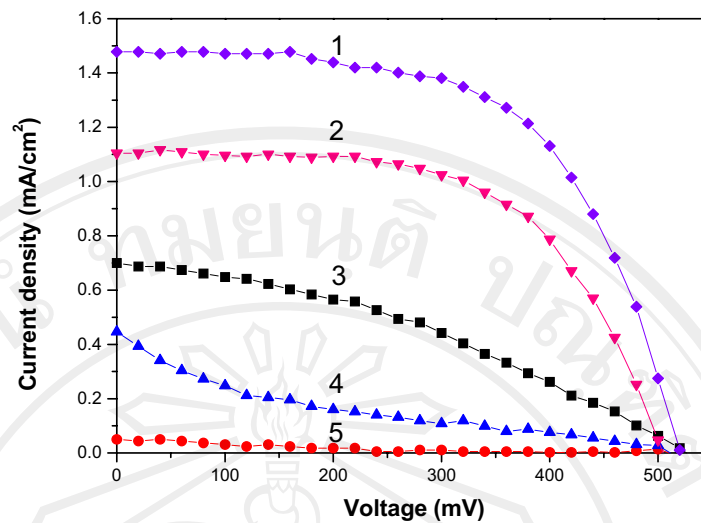


Figure 4.23 J-V characteristics of ZnO DSSCs with different photoelectrodes-counter-electrodes (1) ZnO/CuO nanowire-Pt, (2) ZnO/CuO powder-Pt, (3) ZnO-Pt, (4) ZnO-CuO nanowire and (5) ZnO-CuO powder.

Table 4.3 Summary of the photoelectrochemical parameters such as J_{sc} , V_{oc} , FF and η determined from the measured J-V curves in figure 4.24.

photoelectrode-counter-electrode	$V_{oc}(V)$	$J_{sc}(mA/cm^2)$	FF	$\eta(\%)$
1. ZnO/CuO nanowire – Pt	0.52	1.49	0.59	0.46
2. ZnO/CuO powder – Pt	0.50	1.11	0.61	0.33
3. ZnO – Pt	0.52	0.70	0.36	0.13
4. ZnO – CuO nanowire	0.51	0.47	0.15	0.03
5. ZnO – CuO powder	0.49	0.12	0.13	0.01

4.4.3 CuO as p-n junction DSSCs

In the previous section, CuO thin films shows highest efficiency of DSSCs when used as a p-n photoelectrode. Here, CuO with difference structure such as nanowires, powder and thin films was studied for used as p-n junction photoelectrode in DSSCs. The difference structure of CuO such as nanowires, powder and thin films was prepared on the top of ZnO for using as a photoelectrode in DSSCs. The

preparation of the p-n junction photoelectrode was shown in the previous chapter. Figure 4.24 showed J-V characteristic of ZnO DSSCs with ZnO/CuO layer as a photoelectrode. For comparison, J-V characteristic of ZnO DSSCs without CuO is also shown in figure 4.24. The photoelectrochemical parameters such as short current density, open circuit voltage, fill factor and the overall power conversion efficiency which determined from the measured J-V curves were summarized in table 4.4.

Clearly, ZnO DSSC with CuO thin film as a barrier layer showed highest short current density of 5.10 mA/cm^2 and highest power conversion efficiency ($\eta = 0.92\%$). This could be explained in terms of low back or reverse current due to the retardation of the interfacial recombination dynamics of CuO blocking layer⁽⁴⁰⁾.

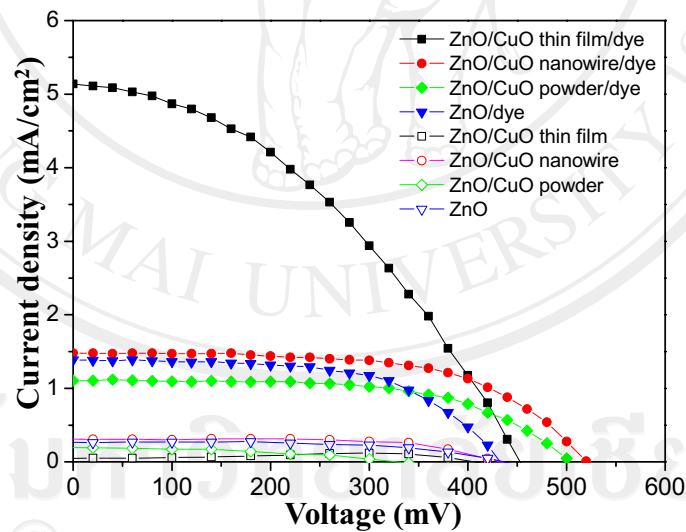


Figure 4.24 Measured J-V characteristic of ZnO DSSCs with ZnO/CuO layer as a photoelectrode.

Table 4.4 Summary of the photoelectrochemical parameters such as J_{SC} , V_{OC} , FF and η determined from the measured J-V curves.

Type of photoelectrode	$V_{OC}(V)$	$J_{SC}(mA/cm^2)$	FF	Eff(%)
ZnO/CuO thin films	0.45	5.10	0.40	0.92
ZnO/CuO nanowire	0.52	1.49	0.59	0.46
ZnO/CuO powder	0.50	1.11	0.61	0.33
ZnO	0.43	1.40	0.62	0.43

4.4.4 Effect of barrier layer on photoelectrochemical characteristics

Charge transfer processes of the Eosin-Y sensitized solar cell based on ZnO are illustrated in Figure 4.22(a). When the Eosin-Y sensitizer absorbs a photon and transform to the excited state, an electron occupies the LUMO of Eosin-Y and the electron can inject to the conduction band of ZnO as



where D^* , D^+ and e_{ZnO} are excited dye, and oxidized dye, respectively. After that, injected electron diffuses through to FTO and flows through the load via the external circuit and then reaches the counterelectrode. At the counterelectrode, the oxidized redox species (R^+) is subsequently reduced back to the R through accepting electron.

R^+ is generated from the chemical reaction is



where D, R and R^+ is an original dye, redox species, and oxidized redox species, respectively. This equation is usually called dye regeneration process. The oxidized dye is quickly reduced back to its original state by reduce redox species (R) in the electrolyte for a complete cycle of electron transfer.

Moreover, the observed photocurrent density is given by

$$J_{ph} = J_{inj} - J_r \quad (4.5)$$

where J_{inj} is the electron injection current resulting from dye sensitization and J_r is the surface recombination current which depends on back electron transfer. The back electron transfer which causes energy-wasting recombination has several possible pathways. Two important pathways are the recombination of with the oxidized dye before the dye can be generated and the recombination of with the oxidized redox species ⁽⁴⁰⁾.

In our case, CuO barrier layer is coated on top of the ZnO photoelectrode. As shown in the energy level diagram in Figure 4.21 (b), the CuO barrier layer prevents electrons from back or reverses transfer to the dye and electrolyte resulting in low back or reverse current. Thus, energy-wasting recombination is less, electron injection process to ZnO is more efficient and finally, short current density is higher.

Normally, the maximum open circuit voltage of ZnO DSSC depends on the difference of the energy level between redox potential of electrolyte and the Fermi-level of ZnO. Thus, the open circuit voltage of ZnO DSSCs is independent of morphology and dye adsorption surface area of ZnO. This is in agreement with our results that open circuit voltage of ZnO DSSC shows similar value for all samples.

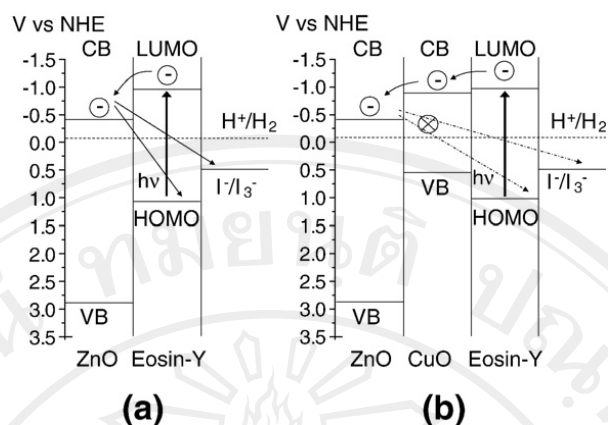


Figure 4.25 Schematic energy level diagram of (a) ZnO-Pt and (b) ZnO/CuO-Pt (p-n junction photoelectrode).

4.4.5 The effect of ZnO passivating layer by sputtering ZnO on FTO in DSSCs

For improving the efficiency of the solar cells, sputtering of ZnO on FTO was used as passivating layer for smoothing contact between the ZnO nanoparticle layer and FTO conducting glass. For this study, the ZnO passivating layer was prepared by sputtering of a ZnO target with different time of sputtering at 5, 10, 20 and 40 min to change the thickness of the passivating layer. The preparation of the photoelectrode was shown in chapter 4.3.2. The effect of passivating layer thickness showed different efficiencies of solar cells. J-V characteristics of DSSC with and without ZnO passivating layer are shown in figure 4.26. The summarized characterization results of DSSCs are shown in table 4.5 and 4.6. Table 4.5 shows the characterization of DSSCs without CuO thin films as a barrier layer. The cells with ZnO passivating layer with sputtering time 5 and 10 min showed higher efficiency of DSSCs than the cell without ZnO passivating layer. However the cells with ZnO passivating layer with sputtering time of 20 and 40 min showed lower efficiency than the cell without ZnO passivating layer. Table 4.6 shows the characterization of DSSCs with CuO thin films as as

barrier layer. The cells with ZnO passivating layer with sputtering time 5 and 10 min showed higher efficiency of DSSCs than the cell without ZnO passivating layer. However the cells with ZnO passivating layer with sputtering time of 20 and 40 min showed lower efficiency than the cell without ZnO passivating layer. Figure 4.26 shows the relationship of DSSCs with and without CuO barrier layer.

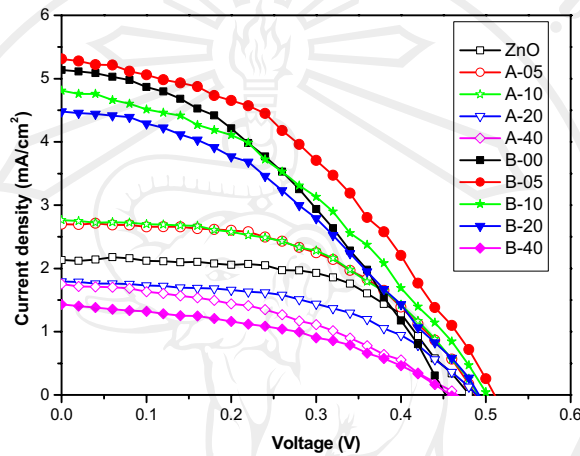


Figure 4.26 J-V characteristic curves of DSSCs.

Table 4.5 Characterization of DSSCs without CuO thin films as a barrier layer

Type	V_{oc} (V)	J_{sc} (mA/cm ²)	FF	η (%)	R_{sh} (Ohm.cm ²)	R_s (Ohm.cm ²)
ZnO	0.47	2.13	0.60	0.60	6790	32
A05	0.48	2.70	0.53	0.68	3601	35
A10	0.48	2.78	0.52	0.69	1293	34
A20	0.48	1.79	0.52	0.44	2064	49
A40	0.46	1.75	0.41	0.33	977	47

Table 4.6 Characterization of DSSCs with CuO thin films as a barrier layer

Type	V_{oc} (V)	J_{sc} (mA/cm ²)	FF	η (%)	R_{sh} (Ohm.cm ²)	R_s (Ohm.cm ²)
B00	0.45	5.10	0.40	0.92	538	37
B05	0.50	5.27	0.42	1.11	527	33
B10	0.49	4.77	0.40	0.94	485	35
B20	0.48	4.47	0.39	0.84	636	36
B40	0.46	1.75	0.41	0.33	864	48

DSSCs with CuO thin films as a barrier layer showed lower FF than DSSCs without CuO thin films as a barrier layer as shown in table 4.5 and 4.6. This may be explained by a decrease of shunt resistance.

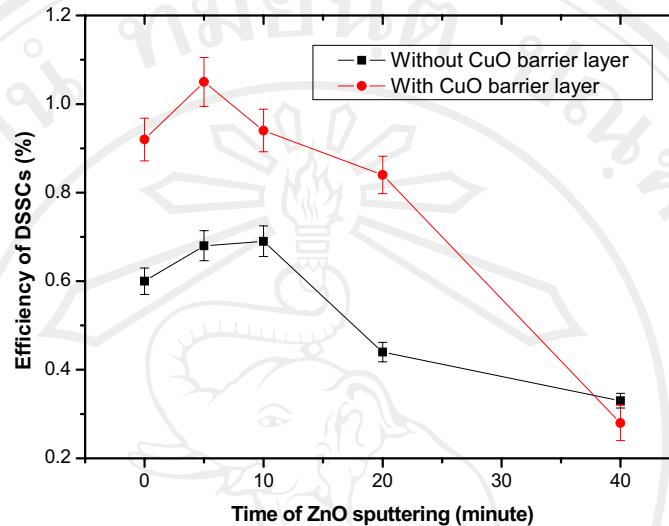


Figure 4.27 The relationship of DSSCs with and without CuO thin films as a barrier layer.

Figure 4.24 showed the efficiency summarized of ZnO DSSCs. The solid square shape is the efficiency of DSSCs with and without sputtering layer with difference thickness was prepared as passivating layer for photoelectrode of DSSCs by without CuO thin films as a barrier layer. The solid circle shape is the efficiency of DSSCs with and without sputtering layer with difference thickness was prepared as passivating layer for photoelectrode of DSSCs by with CuO thin films as a barrier layer. For the efficiency of solar cells without CuO thin films as a barrier layer, the cells with sputtering time of 5 and 10 min show higher efficiency than standard DSSCs was prepared from ZnO as photoelectrode. However the efficiency of DSSCs with sputtering ZnO passivating layer show lower efficiency than ZnO photoelectrode when sputtering time was increased to 20 and 40 min.